Damping Synthesis from Substructure Tests

T. K. Hasselman*
J. H. Wiggins Company, Redondo Beach, Calif.

A new method is proposed for synthesizing structural damping from substructure test data. It utilizes the off-diagonal coupling terms in the substructure modal damping matrices as well as the diagonal terms which correspond to uncoupled modal damping. The coupling terms are evaluated from complex resonant response measured at each substructure mode. Both analytic and experimental verification of the method have been made. Tentative accuracy requirements on experimental data and data reduction are suggested.

I. Introduction

THE treatment of damping in complex structures has always posed difficult problems. Owing to the variety of different mechanisms that contribute to damping and to the general lack of knowledge regarding many of them, it has not been possible to model damping on a finite element basis the way mass and stiffness are modeled. For the most part, structural damping is specified in terms of modal damping, which must be determined experimentally. The advantage of this approach is that one need not be concerned about where damping comes from as long as its influence on response is known. To measure modal damping, the entire structure is usually excited to resonance. There are practical limits to conducting full-scale dynamic tests on some structural systems. Large space vehicles, such as the shuttle, and nuclear reactor systems are difficult to test because of their size. Spacecraft with their appendages deployed may not only be too large, but also too weak to test in a 1-*g* environment. An alternative procedure based on combining substructure damping characteristics is the subject of this paper.

The term "modal damping" usually refers to the fraction of critical damping or the modal damping ratio for a particular natural mode of structural vibration. It can be determined in various ways by measuring the rate of amplitude decay in free vibration, the bandwidth of the frequency response function near resonance, or the rate at which the phase angle of response changes as the frequency of sinusoidal excitation is swept through resonance.

A more complete representation of modal damping is provided by the *full modal damping matrix*. The diagonal elements of this matrix have a one-to-one correspondence with the modal damping ratios of each mode.[1] The off-diagonal elements couple the "classical"† modes of the structure. Only under special conditions are the equations of motion completely diagonalized by the classical modal transformation,[2] and these conditions, appear to have little physical justification. In general, and evidentally for most real structures, modal damping matrices are not diagonal, and the off-diagonal terms may be of the same order of magnitude as the diagonal terms.[1,3]

Frequently in structural dynamic analysis, the modal coupling terms can be ignored. If one is considering a structural system whose linearized damping matrix is transformed to a modal damping matrix by the classical modes of the system, then the modal coupling terms are only important when two or more modes of the system have such close frequencies that the small damping forces in the system pass significant amounts of energy from one mode to another.[4]

In the case of damping synthesis, a quite different situation prevails. When a system mode is comprised of several subsystem modes *from each subsystem*, the modal coupling terms for those subsystems cannot be ignored. To do so may introduce significant error in the dissipative energy computed for that system mode, so that the corresponding modal-damping ratio will be in error. The proposed method for damping synthesis utilizes these coupling terms and demonstrates how they may be derived from experimental data.

Except for the evaluation of substructure modal damping matrices, the procedure used to synthesize system damping from substructure data is common to many previous investigations. The modal synthesis transformation is applied to component damping matrices in the same way it is applied to component mass and stiffness matrices. The procedure is shown in Fig. 1. The conventional approach entails the following steps:

Determine the classical modes of each substructure using resonant response data. Phase separation techniques may be used to improve the resolution of these modes.

Determine substructure modal frequencies and damping ratios, and generate diagonal modal damping matrices.

Perform modal synthesis using the undamped equations of motion, obtaining the modal synthesis transformation.

Compute system damping by pre- and postmultiplying the diagonal substructure damping matrices by the modal synthesis transformation matrix. The diagonal elements of the resulting system damping matrix correspond to the system modal damping ratios.

It is evident from Fig. 1 that these four steps correspond to Steps 1, 2, 4, and 5 of the proposed method. The only one missing is Step 3 in which the full modal damping matrices are obtained to use in place of the diagonal ones. In the process of doing this, the measured substructure modes are further

Presented as Paper 74-387 at the AIAA/ASME/SAE 15th Structures, Structural Dynamics and Materials Conference, Las Vegas, Nev., April 17-19, 1974; submitted April 26, 1974; revision received June 14, 1976. The majority of the work reported in this paper was performed at TRW Systems and sponsored by the NASA Langley Research Center under Prime Contract Number NAS1-10635, and was performed under subcontract to the Grumman Aerospace Corp., Contract Number 0-16232-c. The cooperation of Robert Fralich, NASA Technical Monitor, and Murry Bernstein, GAC Technical Monitor, is gratefully acknowledged. Key contributions to the study were made by Robert Herr of Langley Research Center who was responsible for conducting all of the tests, Charles P. Wright of TRW for analog data reduction, and Stephen Goldenberg of GAC for developing the modal synthesis transformations. The author wishes to acknowledge support by the J. H. Wiggins Co. in preparation of the original manuscript, and the final manuscript, which was substantially rewritten.

Index categories: Aircraft Vibration; Spacecraft Ground Testing and Simulation (Including Components); Structural Dynamic Analysis.

*Manager, Engineering Mechanics Department. Member AIAA.

†Classical modes are defined to be those *real* modes that diagonalize the mass and stiffness matrices.

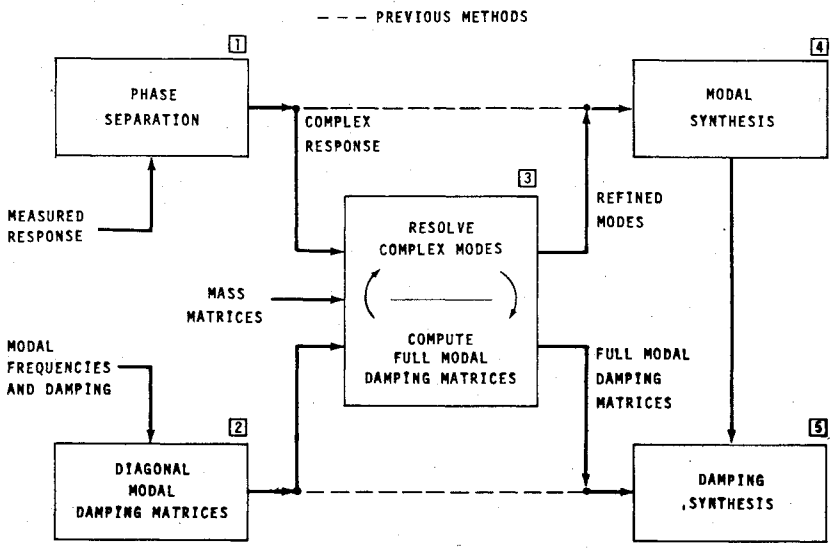

Fig. 1 Flow diagram for damping synthesis procedure. Dashed lines indicate the conventional approach.

refined. The details of this method are presented in the sections that follow.

II. Damping Synthesis

The various coupling procedures currently used for modal synthesis depend on the type of substructure modes used. From the standpoint of damping synthesis, the basic equations are the same. Without going into detail, the general procedure may be outlined rather simply.

Equations of motion written in terms of discrete physical coordinates for a set of unconnected components are of the form

$$\mu\ddot{x}+\rho\dot{x}+\kappa x=f \tag{1}$$

where the square matrices μ, ρ, and κ are all of block diagonal form and the vector f contains interactive forces between components.

There are three transformations involved in going from Eq. (1) to a reduced set of equations in system modal coordinates. The first transformation, denoted by ϕ_R, involves the classical substructure modes. The subscript R is used to signify that these modes are real. The transformation may be written

$$x=\phi_R p \tag{2}$$

The second transformation is a rectangular matrix denoted by β, and is used to introduce compatibility constraints at substructural interfaces. The final transformation Φ_R involves the classical modes of the *system*, where each column of Φ_R is a system eigenvector in the coupled component mode coordinates. These latter two transformations relate the p coordinate vector to a new coordinate vector η, whose elements correspond to the system eigenvectors Φ_R. Thus

$$p=\beta\Phi_R\eta=T\eta \tag{3}$$

It is convenient both conceptually and notationally to combine β and Φ_R into the single matrix T referred to as the *modal synthesis transformation matrix*. Transformation of Eq. (1) to the η coordinate system gives equations of the form

$$I\ddot{\eta}+C\eta+\Omega_0^2\eta=f_\eta \tag{4}$$

when Φ_R is normalized to give unit modal mass. In other words

$$T^T\phi_R^T\mu\phi_R T\equiv I \tag{5a}$$

$$T^T\phi_R^T\rho\phi_R T=C \tag{5b}$$

$$T^T\phi_R^T\kappa\phi_R T=\Omega_0^2 \tag{5c}$$

where I is an identity matrix, Ω_0^2 is a diagonal matrix of undamped system frequencies squared, and C is, in general, a fully populated modal damping matrix at the system level.

The off-diagonal elements of C are usually neglected,[4] whereas the diagonal elements, according to Ref. 1 are given by

$$C_{jj}=2\zeta_j\Omega_{0_j} \tag{6}$$

ζ_j being the critical damping ratio for the jth mode. Without full-scale testing of the composite structure, ζ_j cannot be obtained directly. The problem then is to find some other means of determining C_{jj}.

In Eq. (5b), it is convenient to let $\phi_R^T\rho\phi_R=c$ where for N components, c is of the block diagonal form

$$c=\begin{bmatrix} c^1 & & & \\ & c^2 & & \\ & & \ddots & \\ & & & c^N \end{bmatrix}$$

and $c^i=\phi_R^{i\,T}\rho^i\phi_R^i$. The scalar C_{jj} may then be expressed in the form

$$C_{jj}=\sum_i T_j^{i\,T}c^i T_j^i \tag{7}$$

where T_j denotes the jth column of T and

$$T=\begin{bmatrix} T^1 \\ \hline T^2 \\ \hline \vdots \\ \hline T^N \end{bmatrix}$$

corresponding to the partitioning of c. Physically, the submatrices T^i represent the contributions of the component modes to the system modes. In other words, each element of the vector T_j^i represents the contribution of one of the modes of the ith component to the system mode, Φ_{R_j}.

III. Dissipative Energy

When a single mode of vibration, say the jth mode, is excited sinusoidally at its resonant frequency Ω_{0_j}, the energy D_j dissipated by the structure during one cycle of vibration is obtained by integrating the product of localized damping forces

and structural velocities over the entire structure for one natural period, τ_j. In matrix form, D_j is then

$$D_j = \int_0^{\tau_j} F_j^T(t)\, v_j(t)\, dt$$

$$= \sum_i T_j^{i\,T} c^i T_j^i \int_0^{\tau_j} \left|\dot{\eta}_j^2(t)\right| dt$$

$$= 2\zeta_j \Omega_{0_j} (\pi M_j \Omega_{0_j} \eta_{0_j}^2) = 4\pi K_j \zeta_j \qquad (8)$$

where

$K_j = \frac{1}{2} M_j \Omega_{0_j}^2 \eta_{0_j}^2$, the modal kinetic energy

$F_j(t) = c v_j(t)$, the vector of damping forces

$v_j(t) = \phi_R T_j \dot{\eta}_j(t)$, the velocity vector

$\eta_j(t) = \sqrt{M_j}\eta_{0_j} \sin\Omega_{0_j} t$, the displacement in the jth modal coordinate of the system

It is recalled from Eq. (3) that $T = \beta\Phi_R$, so that T may be obtained by solving the undamped modal synthesis problem. To determine D_j, the component modal damping matrices c^i for each component i, must be obtained. It is clear from Eqs. (7) and (8) that the off-diagonal terms of c^i cannot be ignored without introducing error in both D_j and ζ_j.

Since the diagonal elements of c^i have a one-to-one correspondence with the modal damping ratios, it must be concluded that *more information is required to determine the off-diagonal elements*. For this reason, methods that use only the modal damping ratios (diagonal terms of the modal damping matrix), e.g., Ref. 5, to characterize substructure damping, are not *generally* applicable to real structures.

IV. Forms of the Substructure Modal Damping Matrix

Identification of substructure damping properties will depend on the type of substructure modes used in the synthesis. The mode types are governed by the boundary conditions imposed. Interface boundaries may be free, fixed, or reflect some intermediate degree of fixity (by application of mass loading, for example as in Ref. 6). The case involving free-interface boundary conditions is the simplest, both conceptually and from an experimental standpoint. In this case, the modal sub-matrix ϕ_R^i corresponding to the ith component will contain rigid body and flexural modes. For free vibration, the modes ϕ_R^i may be partitioned to distinguish between the rigid body and flexural (normal) modes.

$$\phi_R^i = \left[\begin{array}{c|c} \phi_R^{iR} & \phi_R^{iN} \end{array}\right] \qquad (9)$$

Relative to the modal coordinates p^i, c^i may be partitioned as

$$c^i = \left[\begin{array}{c} \phi_R^{iR\,T} \\ \hline \phi_R^{iN\,T} \end{array}\right] [\rho^i] \left[\begin{array}{c|c} \phi_R^{iR} & \phi_R^{iN} \end{array}\right] = \left[\begin{array}{c|c} c^{iRR} & c^{iRN} \\ \hline c^{iNR} & c^{iNN} \end{array}\right] \qquad (10)$$

In the absence of external damping,

$$c^i = \left[\begin{array}{c|c} 0 & 0 \\ \hline 0 & c^{iNN} \end{array}\right] \qquad (11)$$

The submatrix c^{iNN} may be determined by the method discussed in Ref. 1. After obtaining all of the c^i matrices, $i = 1\text{-}N$, modal damping for the coupled system can be determined by Eq. (7). For mass-loaded interface modes, the form of c^i is also given by Eq. (10).

When fixed-interface substructure modes are used, the determination of c^i will be more difficult. In this case, ϕ_R^i may include three different types of modes – rigid body, constraint, and normal modes. The constraint modes appear only for redundantly interconnected substructures and are introduced so that the motion of interface boundary points is completely defined. These modes are usually chosen to be static deformation shapes obtained by displacing each boundary coordinate sequentially while holding all others fixed and applying no loading whatsoever at points other than attachment points. Under these conditions, ϕ_R^i may be partitioned in the manner

$$\phi_R^i = \left[\begin{array}{c|c|c} \phi_R^{iRB} & I & 0 \\ \hline \phi_R^{iRI} & \phi_R^{iC} & \phi_R^{iN} \end{array}\right] \qquad (12)$$

where ϕ_R^{iRB} is the portion of rigid body modes corresponding to boundary points, ϕ_R^{iRI} is the complementary part corresponding to internal points, I is an identity matrix, ϕ_R^{iC} defines the static deformation shapes of the substructure internal to its interface boundary, and ϕ_R^{iN} represents the fixed boundary normal modes.

The symmetric matrix c^i is then of the form

$$c^i = \left[\begin{array}{c|c|c} c^{iRR} & c^{iRC} & c^{iRN} \\ \hline c^{iCR} & c^{iCC} & c^{iCN} \\ \hline c^{iNR} & c^{iNC} & c^{iNN} \end{array}\right] \qquad (13)$$

From the standpoint of damping, it is apparent that both the free-interface mode method and the fixed-interface mode method suffer from the same basic limitation: the representation of damping *near*‡ interface boundaries may be poor. In the free-interface mode case, the tendency is caused by the fact that the convergence of system modes is slow, with many substructure modes required to attain good accuracy. This is usually explained by the failure of lower frequency modes to adequately "work" the local structure *near* interface boundaries. If strain energy in this region is not properly accounted for, it is likely that the dissipative energy will not be either.

In some respects, the problem associated with using fixed-interface modes for damping synthesis is similar. Displacements near interface boundaries are defined by static displacement shapes for which damping information is not available. So again, the basic problem is an inadequate representation of the structure's dissipative properties *near* substructural interface boundaries.

On the other hand, the use of mass-loaded§ interface modes can potentially overcome this problem. Mass loading causes the structure to be "worked" more in these local areas. It is felt that the dissipative properties of the structure are therefore represented more fully. Selection of the proper mass loading is important, however, and practical difficulties may arise. This topic is discussed in Ref. 6. The damping matrices in this case are of the same form as in the free-interface mode case, so their evaluation is straightforward.

The present application is based on the use of free-free modes. In this particular case, convergence was found to be reasonably good.

V. Computing a Modal Damping Matrix from Damped Modes

In searching for a way to more fully describe the damping properties of a structure, two things become apparent. The first is that most structures tend to be lightly damped; therefore, damped modes closely resemble the hypothetical undamped modes except for small differences in phase. The second is that phase separation techniques presently employed

‡Damping *at* (as distinguished from *near*) a boundary due to bolted or riveted joints for example, must be treated separately. This will require additional information such as specific knowledge of interface damping mechanisms. This topic is not treated in the present paper.

§Lumped masses are attached at component interface boundaries for component testing. This additional mass is later removed analytically during the synthesis operation.

in vibration testing are potentially capable of yielding these small phase differences quantitatively. This phase information can be used to derive a more complete set of structural damping information than simple decay tests provide.

Intuitively, one would expect that if the damping in a structure could be gradually reduced to zero, the damped modes would approach the undamped modes in some continuous fashion. Thus, a damped mode might be representable by a linear perturbation of the corresponding undamped mode. This thinking led to the formulation of the perturbation analysis contained in Ref. 1. The results of this derivation are extended for the present application.

The modal damping matrix c^i may assume different forms, as suggested by Eqs. (10) and (13). The main objective is to determine the submatrix c^{iNN}, which appears in both equations. For convenience, Eqs. (10) and (13) may be put in the same form by writing both Eqs. (9) and (12) as

$$\phi_R^i = [\phi_R^{iB} \vdots \phi_R^{iN}] \tag{14}$$

With this partitioning, the equations of motion in modal coordinates for the ith substructure become

$$\begin{bmatrix} m^{iBB} & m^{iBN} \\ m^{iNB} & m^{iNN} \end{bmatrix} \begin{Bmatrix} \ddot{p}^{iB} \\ \ddot{p}^{iN} \end{Bmatrix} + \begin{bmatrix} c^{iBB} & c^{iBN} \\ c^{iNB} & c^{iNN} \end{bmatrix} \begin{Bmatrix} \dot{p}^{iB} \\ \dot{p}^{iN} \end{Bmatrix} + \begin{bmatrix} k^{iBB} & k^{iBN} \\ k^{iNB} & k^{iNN} \end{bmatrix} \begin{Bmatrix} p^{iB} \\ p^{in} \end{Bmatrix} = \begin{Bmatrix} f_p^{iB} \\ f_p^{iN} \end{Bmatrix}$$

Then one may write

$$m^{iNN}\ddot{p}^{iN} + c^{iNN}\dot{p}^{iN} + k^{iNN}p^{iN} = \bar{f}_p^{iN} \tag{15a}$$

where, in general,

$$\bar{f}_p^{iN} = f_p^{iN} - m^{inB}\ddot{p}^{iB} - c^{iNB}\dot{p}^{iB} - k^{iNB}p^{iB} \tag{15b}$$

Whenever

$$\phi_R^{iN\,T}\mu^i\phi_R^{iN} \equiv I$$

by proper normalization of ϕ_R^{iN}, Eq. (15) is of the special form

$$I\ddot{q} + \xi\dot{q} + \omega_0^2 q = f_q \tag{16}$$

where ω_0^2 is a diagonal matrix of undamped frequencies squared, and ξ is the mass-normalized modal damping matrix.

From this point on, it will simplify the notation considerably to *drop the superscript notation* used to distinguish different substructures and different classes of modes for a given substructure. It will follow, for example, that $x^i = x$, $\mu^i = \mu$, and $\phi_R^{iN} = \phi_R$. With the simplified notation, complex eigenvalues of the form

$$\lambda_j = \sigma_j + i\omega_j \tag{17}$$

are defined. The term $\sigma_j = -\zeta_j\omega_{0_j}$ is interpreted as the decay rate associated with mode j, whereas

$$\omega_j = \omega_{0_j}\sqrt{1-\zeta_j^2}$$

is the damped natural frequency of that mode. The corresponding damped eigenvectors are

$$\phi_j = \phi_{R_j} + \delta\phi_{R_j} + i\delta\phi_{I_j} \tag{18}$$

where ϕ_{R_j} are the undamped modes and $\delta\phi_{R_j}$ and $\delta\phi_{I_j}$ are considered to be small compared to ϕ_{R_j}. For lightly damped structures, the small perturbation assumptions

$$|\sigma_j| << \omega_j$$

$$|\delta\phi_{R_j}|, |\delta\phi_{I_j}| << |\phi_{R_j}|$$

$$|<<|$$

lead to[1]

$$\xi_{jk} = -\delta_{jk}(\sigma_j + \sigma_k) - (\omega_j - \omega_k)(\phi_{R_j}^T\mu\delta\phi_{I_k} - \delta\phi_{I_j}\mu\phi_{R_k}) \tag{19}$$

where δ_{jk} is the Kronecher delta ($\delta_{jk} = 1$, $j=k$; $=0$, $j\neq k$). To clarify physical interpretation, $\delta\phi_{I_j}$ may be expressed as a linear combination of the real modes, ϕ_R. Thus

$$\delta\phi_{I_j} = \sum_k \phi_{R_k}\alpha_{kj} = \phi_R\alpha_j \tag{20}$$

Due to orthogonality of the real modes, it is apparent that

$$\delta\phi_{I_j}\mu\phi_{R_k} = \alpha_j^T\phi_R^T\mu\phi_{R_k} = \alpha_{kj}$$

Therefore,

$$\xi_{jk} = -\delta_{jk}(\sigma_j + \sigma_k) - (\omega_j - \omega_k)(\alpha_{jk} - \alpha_{kj}) \tag{21}$$

Since $\sigma_j = -\zeta_j\omega_{0_j}$, it is seen that

$$\xi_{jj} = 2\zeta_j\omega_{0_j}$$

Finally, it can be shown that to first-order approximation

$$\alpha_{jj} = 0 \tag{22a}$$

$$\alpha_{kj} = \omega_j\xi_{kj}/(\omega_j^2 - \omega_k^2) \qquad k\neq j \tag{22b}$$

It is of interest to note that the perturbation analysis preceding and in Ref. 1 is not strictly dependent on the assumption of a linear viscous damping model. Similar results have been obtained for the complex elastic modulus damping model sometimes referred to as "structural damping."

VI. Separation of Damped Modes from Complex Resonant Response

In a practical sense, the damped modes are not directly measurable from vibration tests because sufficiently "pure" modes are not usually excited. Off-resonant modes may contribute significantly to the total *acceleration* response, particularly in the coincident component defined to be in phase with the forcing function. The quadrature component leads the force by 90° and is normally used to define the classical modes. The fact that off-resonant mode response tends to be relatively small and out-of-phase with that of the resonant mode has provided the basis for phase separation techniques now used to more accurately define the classical modes; however, contamination of the coincident response by off-resonant mode participation imposes the need for modal separation if the damped modes are to be determined at all. An iterative procedure has been developed and demonstrated. For damping levels on the order of 1%, convergence has been achieved in only one or two iterations, although the process may be cycled any number of times should convergence proceed more slowly.

The basic technique to be used for mode separation requires, in addition to resonant response, frequencies, and damping rates, a knowledge of the force input to the structure. Assuming that the quadrature component of each resonant response is a reasonably accurate representation of the classical mode associated with that frequency, the extent of off-resonant mode participation can be determined to good approximation and subtracted from the total response, leaving an improved representation of the resonant mode. This procedure was successfully applied by Stahle[7] more than

a decade ago to improve upon the classical modes of a structure. The present work extends that method for application to the damped modes that are complex. The generalization is valid provided that the structure is lightly damped. Specific validity criteria that involve quantitative relationships among the distribution of the forcing function, the amount of damping, frequency separation of the modes, and measurement accuracy are derived in the Appendix. In keeping with the simplified notation, the equations that follow may be considered to apply to a substructure even though the superscripts are dropped for notational convenience.

The forced equations of motion for a given substructure are first written in the form of Eq. (1). The matrices μ, ρ, and κ are not block diagonal when they apply to a *single* substructure.

To make this development applicable to free-free structures as well as constrained structures, it will be assumed that the displacement vector x defines flexural deformations relative to rigid body motion. In the free-free case, this implies that to utilize total response measurements, rigid body response must first be computed independently and subtracted from the total response.

Under these conditions, the equations of motion as given by Eq. (1) may be transformed by a modal matrix ϕ_R, where in this case ϕ_R contains only undamped flexural modes. Then Eq. (1) becomes

$$I\ddot{q}+\xi\dot{q}+\omega_0^2 q=\phi_R^T f(t)=f_q(t) \tag{23}$$

which is similar in concept and identical in form to Eq. (16). The force vector $f(t)$ will include any forces which couple the elastic modes to other modes, as indicated by Eq. (15b). It is assumed that, in general, a different force vector $\bar{f}(t)$ will be generated to exicte resonant response at each natural frequency Ω_j, and consequently, that

$$\bar{f}(t)=\bar{P}_{x_j} g_j(t) \tag{24}$$

The complex frequency response vector corresponding to Ω_j is then given by

$$H_{q_j}=[(\omega_0^2-\Omega_j^2 I)+i\Omega_j\xi]^{-1}\phi_R^T\bar{P}_{x_j} \tag{25}$$

Initially, it may be assumed (neglecting off-diagonal terms) that

$$\xi_{jk}=-\delta_{jk}(\sigma_j+\sigma_k)$$

where δ_{jk} is the Kronecker delta, and that ϕ_R is approximated by the normalized quadrature component of acceleration response. Thus, a vector H_{q_j} may be evaluated for each of the resonant response conditions and transformed back to the x coordinate system by

$$H_{x_j}=\phi_R H_{q_j}$$

Combining these equations in a single matrix equation gives

$$H_x=\phi_R H_q$$

where H_q is assumed to be a nonsingular square matrix. Then,

$$\phi_R=H_x H_q^{-1} \tag{26}$$

provides the first *refined* estimate of the real modes ϕ_R. The vector H_{x_j} is obtained from the complex (both real and imaginary) acceleration response data.

To derive an estimate of $\delta\phi_I$, Eq. (1) is written in the first-order form

$$\left[\begin{array}{c|c}\rho & \mu\\ \hline \mu & 0\end{array}\right]\left\{\begin{array}{c}\dot{x}\\ \hline \ddot{x}\end{array}\right\}+\left[\begin{array}{c|c}\kappa & 0\\ \hline 0 & -\mu\end{array}\right]\left\{\begin{array}{c}x\\ \hline \dot{x}\end{array}\right\}=\left\{\begin{array}{c}f(t)\\ \hline 0\end{array}\right\}$$

Solution of the corresponding first-order eigenproblem leads to the transformation

$$\left\{\begin{array}{c}x\\ \hline \dot{x}\end{array}\right\}=\left[\begin{array}{c|c}\phi & \phi^*\\ \hline \phi\lambda & \phi^*\lambda^*\end{array}\right]\left\{\begin{array}{c}z\\ \hline \end{array}\right\}$$

where asterisks denote the complex conjugate. The frequency response vector in the z coordinate system is then given by

$$H_{z_j}=\left[\begin{array}{c|c}(i\Omega_j I-\lambda) & 0\\ \hline 0 & (i\Omega_j I-\lambda^*)\end{array}\right]\left[\begin{array}{c|c}A & 0\\ \hline 0 & A^*\end{array}\right]^{-1}\left[\begin{array}{c}\phi^T\\ \hline \phi^{*T}\end{array}\right]\bar{P}_{x_j} \tag{27}$$

where A is a diagonal matrix whose elements are obtained from the equation

$$A_j=\phi_j^T\rho\phi_k+\phi_j^T\mu\phi_k\lambda_k+\lambda_j\phi_j^T\mu\phi_k \tag{28}$$

and a first-order perturbation analysis using Eqs. (17) and (18) which leads to

$$A_j=i2\omega_j \tag{29}$$

Assuming that ϕ in Eq. (27) may be approximated by the real part of the resonant response matrix, one may evaluate a vector H_{z_j} for each resonant frequency and relate it to response in the x coordinate system by

$$H_{x_j}=[\phi\,\vdots\,\phi^*]H_{z_j} \tag{30}$$

Combining these equations for each resonant response, j, into a single matrix equation gives

$$H_x=[\phi\,\vdots\,\phi^*]H_z \tag{31}$$

Alternatively, recognizing that ϕ and ϕ^* may be expressed in terms of $\phi_R+\delta\phi_R\approx\phi_R$, and $\delta\phi_I$, one may write

$$H_x=\phi_R H_R+\delta\phi_I H_I \tag{32}$$

where H_R and H_I are both complex square matrices derived from H_z. Having already found ϕ_R from Eq. (26), $\delta\phi_I$ is given by the equation

$$\delta\phi_I=(H_x-\phi_R H_R)H_I^{-1} \tag{33}$$

With ϕ_R and $\delta\phi_I$ computed, the first iteration is complete. To begin the second iteration, these values are used in Eq. (19) to update the matrix ξ. Then Eqs. (25-33) may be recycled to complete the second iteration. Succeeding iterations follow in the same way. The entire procedure may be summarized by the following:

Initial Values

Define the damped modes initially by the quadrature acceleration response QUAD($H_{\ddot{x}}$). That is,

Step 0: $\phi_j=\text{QUAD}(H_{\ddot{x}_j})/[\text{QUAD}(H_{\ddot{x}_j})^T\mu\,\text{QUAD}(H_{\ddot{x}_j})]^{1/2}$

These vectors are defined to be real, and are of the form $\phi_j=\phi_{R_j}$; the imaginary parts $\delta\phi_{I_j}\equiv 0$.

Evaluate Matrices ξ and A

Step 1: $\xi_{jk}=-\delta_{jk}(\sigma_j+\sigma_k)-(\omega_j-\omega_k)(\alpha_{jk}-\alpha_{kj})$

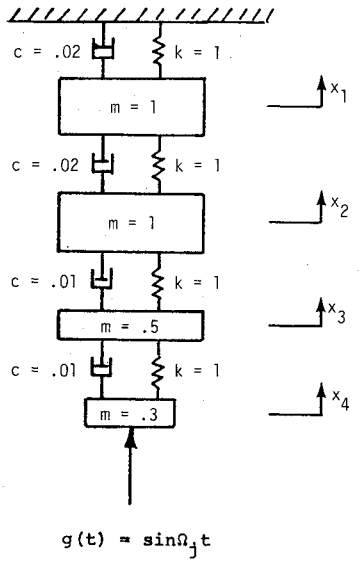

Fig. 2 Analytic lumped parameter model.

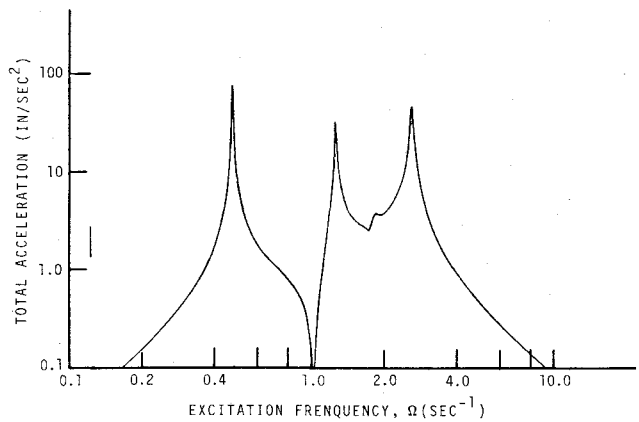

Fig. 3 Acceleration response for mass number 3.

Step 2: $A_j = i2\omega_j$

Compute the Real and Imaginary Parts of the Damped Modal Matrix

Step 3: $H_{q_j} = [\,(\omega_0^2 - \Omega_j^2 I) + i\,\Omega_j \xi\,]^{-1} \phi_R^T \bar{P}_{x_j}$

(in first iteration, $\phi_R = \phi$ from step 0).

Step 4: $\phi_R = H_x H_q^{-1}$

Step 5:

$$H_{z_j} = \left[\begin{array}{c|c} (i\,\Omega_j I - \lambda) & 0 \\ \hline 0 & (i\,\Omega_j I - \lambda^*) \end{array}\right] \left[\begin{array}{c|c} A & 0 \\ \hline 0 & A^* \end{array}\right]^{-1} \left[\begin{array}{c} \phi^T \\ \hline \phi^{*T} \end{array}\right] \bar{P}_{x_j}$$

Step 6: $H_x = [\phi \vdots \phi^*] H_z \approx \phi_R H_R + \delta\phi_I H_I$

Step 7: $\delta\phi_I = (H_x - \phi_R H_R) H_I^{-1}$

Steps 1 through 7 may be repeated any number of times. The procedure should converge if the proper conditions are met. Again, these conditions are derived in the Appendix.

VII. Analytical Verification¶

To demonstrate the use of resonant response data in computing a modal damping matrix, the idealized lumped parameter system shown in Fig. 2 was considered. Simulated response data were generated using the mass, stiffness, and damping information shown in Fig. 2. These data included complex acceleration response functions for each of the four masses. An example of the total acceleration *amplitude* for Mass Number 3 is shown in Fig. 3. Modal frequencies and damping ratios were determined by solving the corresponding first order (complex) eigenvalue problem. These values were also used as part of the simulated test data. Thus, to simulate the data obtainable from test, the total response for each resonant mode was used, along with modal frequencies and damping ratios. *The complex eigenvectors were not used.*

Modal damping matrices were computed by the procedure described earlier, using all four of the resonant modes. Then, the effect of using truncated modal information was investigated using only three and then two of the lower frequency resonant response vectors. The results of these computations are shown in Table 1 where the three computed damping matrices are compared to the reference modal damping matrix $c = \phi_R^T \rho \phi_R$.

¶This example pertains to one component of a system. It is meant to demonstrate the procedure derived in Sec. V and VI.

The agreement is seen to be quite good except for the fourth column of the matrix where deviations are as large as 18%. These are believed to result from phase angle sensitivity in the neighborhood of resonance, indicating the need for accurate measurement of excitation frequencies at resonance, and perhaps, independent determination of modal frequencies. Since the phase angle of response is critically dependent on the difference between these two frequencies squared, care must be taken either to excite the structure at precisely its modal frequency in which case the difference will be zero, or to determine both frequencies precisely (to five significant figures). The latter may be achievable using procedures suggested by Kennedy and Pancu.[8] Further investigation is warranted.

The results of modal truncation showed that very good estimates of reduced modal damping matrices were achieved using incomplete sets of lower frequency modes. Since in practice one will always be working with an incomplete set of modes, this is an important consideration.

VIII. Experimental Verification

The chief purpose of the referenced study[3] was to apply the present method for damping synthesis to a real structural system and compare predicted values of system modal damping with those obtained by direct measurement. This was accomplished by using modal test data furnished by the NASA Langley Research Center. Component and system test data were obtained for a 1/15th scale dynamic model of an early shuttle configuration. This consisted of two separate tubular substructures, an orbiter and a booster model, with lead weights attached to simulate propellant loading. Artificial external damping was added to the orbiter substructure for both component and system level tests. All tests were conducted in the free-free condition. Component tests were performed with the orbiter and booster suspended horizontally, whereas the system tests were performed with the assembly suspended vertically. For the system test, the orbiter and booster components were redundantly interconnected by three special spring assemblies incapable of transmitting moment, i.e., three pinned connections. The configuration is shown schematically in Fig. 4.

Because of the external damping, the discrete damping coefficients were required to evaluate the generalized modal forces in Eq. (15b). This also provided an alternative means for computing the orbiter modal damping matrix. Three *identical* dampers were used, each consisting of a wooden ball attached to the orbiter and inserted into a glass (baby food) jar fixed to ground. Each jar was filled with Dow Corning

Table 1 Comparison of modal damping matrices for analytical model

Reference: $c=\phi_R^T\rho\phi_R$

$$c=\begin{bmatrix} 4.17 & -1.41 & -1.34 & .633 \\ & 21.2 & -9.06 & 1.45 \\ & & 51.58 & -4.28 \\ \text{sym.} & & & 66.3 \end{bmatrix} \times 10^{-3}$$

Computed: 4 modes

$$c=\begin{bmatrix} 4.17 & -1.42 & -1.28 & .748 \\ & 21.2 & -8.94 & 1.61 \\ & & 51.58 & -4.21 \\ & & & 66.4 \end{bmatrix} \times 10^{-3}$$

Computed: 3 modes

$$c=\begin{bmatrix} 4.17 & -1.42 & -1.36 \\ & 21.2 & -8.85 \\ & & 51.6 \end{bmatrix} \times 10^{-3}$$

Computed: 2 modes

$$c=\begin{bmatrix} 4.17 & -1.41 \\ & 21.2 \end{bmatrix} \times 10^{-3}$$

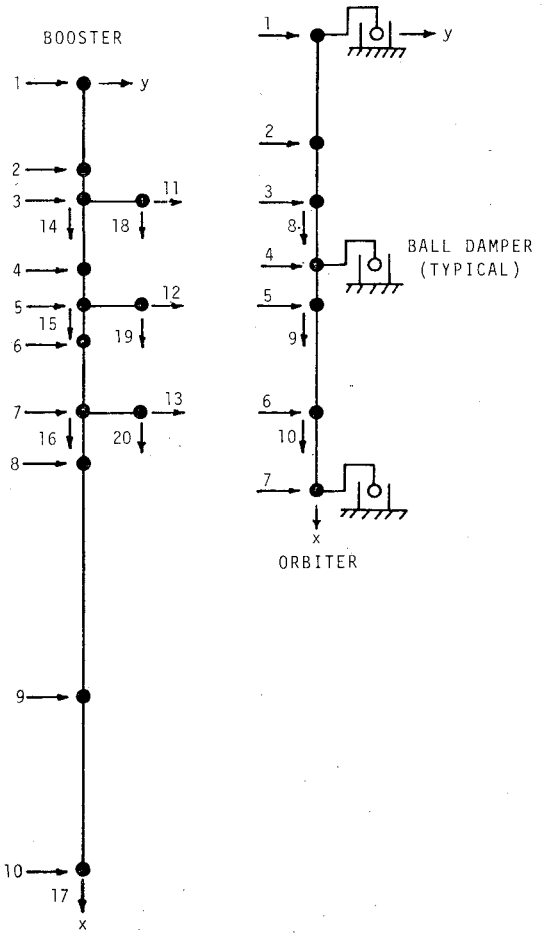

Fig. 4 Schematic representation of a shuttle configuration.

damping fluid having a viscosity of 20 K centistokes so that the balls were totally immersed in the fluid. Tests were run for a typical damper to determine its damping characteristics for both horizontal and vertical ball motion. Linear dependence of the damping forces with respect to velocity was established and a reasonably *constant ratio* of vertical to horizontal damping was demonstrated for frequencies up to about 200 Hz.

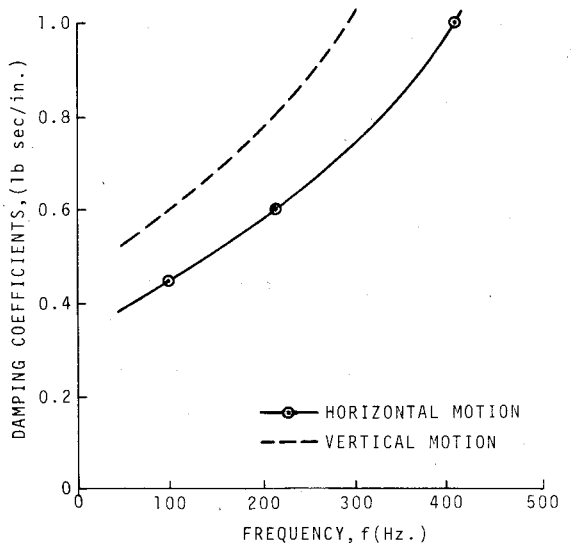

Fig. 5 Damping characteristics for the ball damper.

Table 2 Measured frequencies and damping for the orbiter

Mode description	Frequency (Hz)	Percent critical damping[a] (a)	(b)	(c)
1st bending	101.40	3.43	3.33	3.78
2nd bending	219.78	2.00	1.90	2.32
3rd bending	414.93	0.75	0.78	0.87

[a](a) Half-power-point bandwidth; (b) log decrement; (c) Kennedy-Pancu

Using the previous information in conjunction with modal damping values obtained from orbiter vibration tests, horizontal and vertical damping coefficients were plotted vs frequency as shown in Fig. 5. Unfortunately, variation with frequency was found to be significant. The only recourse was to use average values in the linearized analyses. Although this undoubtedly introduced some degree of error into the computations, it should be recognized that the problem arose as a direct result of using artificial dampers and would not be encountered in actual practice.

Based on free-free component vibration tests run separately for the orbiter and booster, resonant frequencies, damping ratios, and corresponding response vectors were obtained. The full modal damping matrix was computed for the orbiter. Since most of the damping in the composite system comes from the orbiter (the damping associated with the booster being small by comparison), only the diagonal part of the modal damping matrix for the booster was evaluated.

In computing the orbiter modal damping matrix, an attempt was made to use three orbiter modes whose frequencies and modal damping ratios are shown in Table 2. However, only the response vectors for the first two modes were accurately determined. The third mode showed large rotational motion of one of the lead weights accounting for about two-thirds of the total orbiter weight, and this motion was not accurately measured. Nevertheless, computations were made and compared to reference values obtained directly from the equation

$$c=\phi_R^T\rho\phi_R$$

where ρ is a diagonal matrix corresponding to the damping coefficients for the discrete external dampers. The results are shown in Table 3. Aslo shown in Table 3 is the 2×2 modal damping matrix obtained by using only the first two orbiter modes.

It may be seen from Table 3 that the coupling term involving the first two modes compares fairly well with that of the reference matrix, both in the three-mode case and the two-mode case. The terms involving the third mode, while bearing some resemblence to the reference matrix, deviated significantly. Mass-orthogonality involving the third mode was also poor.

Modal frequencies and damping ratios obtained for the free-free booster are shown in Table 4. In addition to the first three bending modes, localized spring modes were also excited. The fact that all six spring modes were obtained is notable. Attempts made to omit some of the higher frequency spring modes led to poor convergence in the synthesis of the undamped equations.

Modal synthesis transformations involving the classical modes were determined by Grumman Aerospace Corporation and furnished in punched card form. These results were used in conjunction with the substructure modal damping matrices to synthesize system modal damping. Two orbiter modes and nine booster modes were included. Direct measurements of system frequencies and damping were obtained by connecting the orbiter and booster together and exciting the composite structure in each of its modes. Predicted (synthesized) values of system frequencies and damping are shown in Table 5 along with experimental results. On the whole, the comparison is favorable except for the fourth mode. The discrepancy here was due to poor agreement between the predicted and measured mode shape. In particular, the tail of the orbiter exhibited large motion in the experimentally determined mode, but practically none in the synthesized mode, contributing to a loss of about 30% in dissipative energy. The disparity shows up in the frequency comparison also where a 6.5% error is indicated. All other frequency errors were less than half of this.

It is of interest to interpret the foregoing results in terms of energy relationships. Using the system modal data shown in Table 5, a plot of dissipative versus kinetic energy has been generated. The results are shown in Fig. 6. It is clear from this example, that no smooth relationship exists between dissipative and kinetic energy. In this case, the treatment described in Ref. 5 would not be applicable.

Table 3 Orbiter modal damping matrix

Reference: $c=\phi_R^T \rho \phi_R$

$$c=\begin{bmatrix} 42.4 & 30.0 & 56.8 \\ & 52.5 & 18.9 \\ \text{sym.} & & 40.7 \end{bmatrix}$$

Computed: 3 modes

$$c=\begin{bmatrix} 42.4 & 37.2 & 128.2 \\ & 52.5 & 8.25 \\ \text{sym.} & & 40.7 \end{bmatrix}$$

Computed: 2 modes

$$c=\begin{bmatrix} 42.4 & 39.9 \\ \text{sym.} & 52.5 \end{bmatrix}$$

Table 4 Measured frequencies and damping for the booster

Mode description	Frequency (Hz)	Percent critical damping[a] (a)	(b)	(c)
1st bending	37.93	–	0.290	0.281
2nd bending	101.62	0.197	0.179	0.181
Spring axial	145.56	0.210	0.198	0.200
Spring-axial	151.05	0.132	0.163	0.142
Spring axial	162.86	0.144	0.144	0.152
3rd bending	183.90	–	(0.300)[b]	–
Spring pitch	211.12	–	(0.200)	–
Spring pitch	220.75	–	(0.200)	–
Spring pitch	224.71	–	0.204	–

[a](a) Half-power-point bandwidth; (b) log decrement; (c) Kennedy-Pancu.
[b]Data unavailable. Values in parentheses were assumed for analysis.

IX. Accuracy Requirements

Since computation of each coupling term, ξ_{jk} is made from phase angle data, the limiting accuracy of phase angle measurements will determine the detectability of ξ_{jk}. For 1% damping, it is estimated that phase angle data accurate to $\pm 0.2°$ or 0.0035 rad will be required, assuming that modal

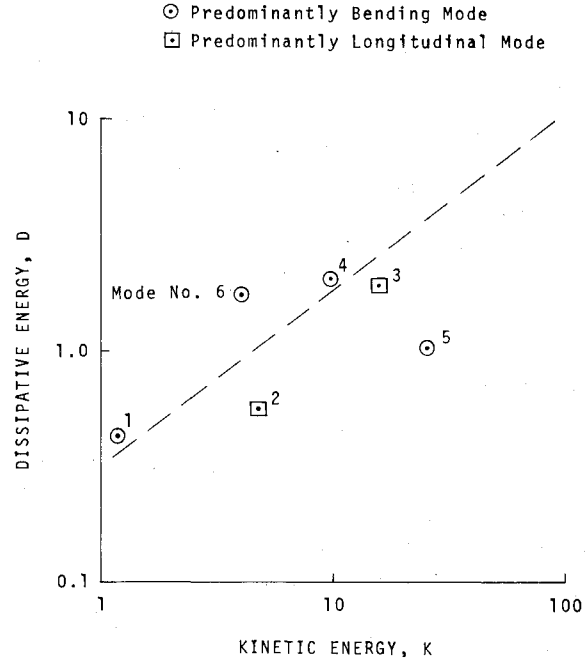

Fig. 6 Energy relationships for the shuttle configuration.

Table 5 Comparison of predicted and measured system modal properties

System mode no.	Modal mass (sec^2/in)	Frequency (Hz) Synthesis	Measured	Damping (%) Synthesis	Measured[a]
1	0.0965	26.4	26.0	3.23	2.77-3.01
2	0.174	38.4	38.7	1.03	0.62-0.96
3	0.309	55.0	57.6	0.66	0.49-0.96
4	0.0595	98.3	92.3	0.77	1.08-1.67
5	0.1275	110.0	108.0	0.31	0.22-0.30
6	0.0139	129.0	125.0	2.98	3.15-3.47

[a]Damping measurements were taken by all three methods. Values span the range indicated.

phase angles are on the order of ζ_j. This will yield approximately a 30% accuracy in ξ_{jk}.

This degree of accuracy was achieved in the present study using analog equipment. A phase-lock control system is recommend to prevent the excitation frequency from drifting and introducing phase shifts. All data were recorded simultaneously on tape for a period of 20-30 sec at a tape speed of 60 ips to minimize the effects of low-frequency flutter. Tape playback was operated in the synchronization mode to compensate for tape deformation. Each channel of data was phase calibrated to compensate for head misalignment.

X. Conclusions

The proposed method for damping syntheis shows promise as a general analytic tool. The theoretical basis has been developed and demonstrated by analytic examples as well as practical application. In addition to verifying the feasibility of the basic approach, the investigation has pointed out directions for further research. They include 1) development of test procedures and equipment for phase control of structural response at resonance, 2) development of more accurate data measurement and reduction capabilities, and 3) development of supplementary analytical procedures for resolving modal data when natural frequencies are closely spaced.

Phase-lock control systems presently available show promise with regard to pursuing the first objective. Digital data acquisition and reduction systems suggest a means of pursuing the second. The use of off-resonant response data in the neighborhood of resonance along with a least-squares type estimator should accomplish the third objective. The theoretical formulation of this approach has been developed and will be published in a later paper. In addition, the question of statistical uncertainty involving the use of measurement data with quantifiable inaccuracies, and the use of lumped parameter models with acknowledged uncertainty, has been considered. A statistical estimator similar to the one presented in Ref. 9 for refining the structural model and determining its modal damping properties has been formulated.

The continued development of this method has thus been well charted. The effort required to pursue the above objectives is by no means trivial. However, the associated costs must be weighed against the potential achievements. No other method known to the author at this time provides a comparable degree of practical applicability and insight for real structures. It is felt that the present method sheds considerable light on the difficult problem of modeling damping in complex structures.

Appendix: Convergence

Convergence of the iterative procedure summarized by steps 1 through 7 of Sec. VI depends on two conditions. The first condition is that Step 0 is valid in the sense that the quadrature component of complex frequency response at each resonant frequency gives a sufficiently accurate approximation of the real part of the corresponding normal mode. This approximation is used to generate ϕ_R in Step 3. If the approximation is not good, then the generalized modal forces $\phi_R^T \bar{P}_{x_j}$ corresponding to each resonant frequency will be erroneous, resulting in incorrect values for H_{q_j}.

As pointed out in Ref. 4, frequency response is insensitive to coupling (off-diagonal) terms in the modal damping matrix ξ as long as the resonant frequencies are sufficiently well-separated. This, then, is the second condition that must be satisfied for convergence. Thus, even though initial values for ϕ_j as derived in Step 0 produce real vectors by definition, and therefore in no way approximate the imaginary part of ϕ_j it doesn't matter as long as the resonant frequencies are spaced far enough apart. This means that ξ_d can be used in place of ξ in Step 3 of the first iteration without introducing appreciable error in H_{q_j}.

While the foregoing paragraphs express the two conditions qualitatively, mathematical expressions can be obtained by first applying a complex scaling transformation to the equation of Step 3 (25), and then using a power series expansion on each term, retaining only the zeroth and first-order terms. The scaling transformation is chosen to be $q = D\gamma$, where

$$D = [(\omega_0^2 - \Omega_j^2 I) + (i\Omega_j)\xi_d]^{-1/2} = Z_d^{-1/2}(i\Omega_j) \tag{A1}$$

as described in Ref. 4. It follows that

$$[I + \tilde{Z}_n(i\Omega_j)]H_{\gamma_j} = P_{\gamma_j} \tag{A2}$$

where

$$\tilde{Z}_n(i\Omega_j) = Z_d^{-1/2}(i\Omega_j) Z_n(i\Omega_j) Z_d^{-1/2}(i\Omega_j)^{-1/2}$$

$$Z_n(i\Omega_j) = i\Omega_j \xi_n$$

$$H_{\gamma_j} = Z_d^{1/2}(i\Omega_j) H_{q_j}$$

$$P_{\gamma_j} = Z_d^{-1/2}(i\Omega_j) P_{q_j}$$

Then

$$H_{\gamma_j} = [I + \tilde{Z}_n(i\Omega_j)]^{-1} P_{\gamma_j} \tag{A3}$$

The matrix $[I + \tilde{Z}_n(i\Omega_j)]^{-1}$ has the series representation

$$[I + \tilde{Z}_n(i\Omega_j)]^{-1} = \sum_{k=0}^{\infty} [-\tilde{Z}_n(i\Omega_j)]^k \tag{A4}$$

provided that the eigenvalues of $\tilde{Z}_n(i\Omega_j)$ are less than unity in magnitude.[10] This condition may be established on the basis of Gershgorin's Disk Theorem, which states that all of the eigenvalues of the complex matrix G lie in at least one of the disks of radius $r_j = \Sigma_k |G_{jk}|$ centered at G_{jj}. Thus the first-order approximation

$$H_{\gamma_j} \approx [I - \tilde{Z}_n(i\Omega_j)] P_{\gamma_j} \tag{A5}$$

may be obtained.

Using similar power series expansions for H_{γ_j} and P_{γ_j} one obtains

$$(H_{\gamma_{0_j}} + \delta H_{\gamma_j}) = [I - \tilde{Z}_n(i\Omega_j)](P_{\gamma_{0_j}} + \delta P_{\gamma_j}) \tag{A6}$$

By equating terms of the same order, one further obtains

$$H_{\gamma_{0_j}} = P_{\gamma_{0_j}} \tag{A7}$$

and

$$\delta H_{\gamma_j} = \delta P_{\gamma_j} - \tilde{Z}_n(i\Omega_j) P_{\gamma_{0_j}} \tag{A8}$$

Thus, in order for δH_{γ_j} to be small compared to $H_{\gamma_{0_j}}$, it is sufficient that δP_{γ_j} be small compared to $P_{\gamma_{0_j}}$, and that the elements of $\tilde{Z}_n(i\Omega_j)$ be small compared to unity. This is the mathematical statement of the two conditions for convergence. It follows after some algebraic manipulation[3] that these conditions reduce to

$$\bar{Q}_{kj} \left| \frac{\hat{\phi}_{R_k}^T P_{x_j}}{\hat{\phi}_{R_j}^T P_{x_j}} \right| << 1 \tag{A9}$$

and

$$(\bar{Q}_{kj})^{1/2} \left| \frac{\xi_{kj}}{\xi_{jj}} \right| << 1 \tag{A10}$$

where

$$\bar{Q}_{kj} = \frac{2\zeta_j(\omega_{0_j}^2/\omega_{0_k}^2)}{\{[1-(\omega_{0_j}^2/\omega_{0_k}^2)]^2 + 4\zeta_k^2(\omega_{0_j}^2/\omega_{0_k}^2)\}^{1/2}} \quad \text{(A11)}$$

Equation (A9) is an expression of the first condition. A frequency separation criterion expressing the second condition is derived from (A10) to be

$$\frac{\omega_{0_k}}{\omega_{0_j}} \geq \left[1+\frac{2\zeta_j}{B^2}\left(\frac{\xi_{kj}}{\xi_{jj}}\right)^2\right]^{1/2} \quad \text{all } j,k \quad \text{(A12)}$$

where $\omega_{0_k} > \omega_{0_j}$, $B << 1$ and where B denotes the largest element of the matrix $\tilde{Z}_n(i\Omega_j)$. In practice, convergence has been achieved for $B \leq 0.2$. Since $\xi_{jj} = 2\zeta_j\omega_{0_j}$, it is evident that the larger ζ_j, the larger the frequency separation must be. Clearly, the smaller the ratio $\xi_{kj}\xi_{jj}$, the closer the frequencies may be spaced.

Since ξ_{kj} is not known at the outset, one may assume $\xi_{kj}/\xi_{jj} \leq 1$, for example. In this case, the frequency separation requirement is

$$\frac{\omega_{0_k}}{\omega_{0_j}} \geq \left[1+\frac{2\zeta_j}{B^2}\right]^{1/2} \quad \text{(A13)}$$

If $\zeta_j = 0.01$ and $B = 0.2$ it is found for example that

$$\omega_{0_k} > 1.225\omega_{0_j}$$

References

[1] Hasselman, T. K., "A Method for Constructing a Full Modal Damping Matrix from Experimental Measurements," *AIAA Journal*, Vol. 10, April 1972, pp. 526-527.

[2] Caughey, T. K., "Classical Normal Modes in Damped Linear Systems," *Journal of Applied Mechanics, ASME Transactions Series E*, Vol. 27, June 1960, pp. 269-271.

[3] Hasselman, T. K., "Study of Modal Coupling Procedures for the Shuttle: A Matrix Method for Damping Synthesis," NASA CR-112253, Dec. 1972.

[4] Hasselman, T. K., "Modal Coupling in Lightly Damped Structures," *AIAA Journal*, Vol. 14, Oct. 1976, pp. xxx-xxx.

[5] Kana, D. D. and Huzar, S., "Syntesis of Shuttle Vehicle Damping Using Substructure Test Results," *AIAA Journal of Spacecraft*, Vol. 10, Dec. 1973, pp. 790-797.

[6] Goldenberg, S. and Shapiro, M., "Study of Modal Coupling Procedures for the Shuttle," *Grumman Aerospace Corporation*, NASA CR-112252, 1972.

[7] Stahle, C. V., Jr., "Phase Separation Techniques for Ground Vibration Testing," *Aerospace Engineering*, July 1962, pp. 408-516.

[8] Kennedy, C. C. and Pancu, C. D. P., "Use of Vectors in Vibration Measurement and Analysis," *Journal of the Aeronautical Sciences*, Vol. 14, Nov. 1947, pp. 603-625.

[9] Collins, J. D., Hart, G. C., Hasselman, T. K., and Kennedy, B., "Statistical Identification of Structures," *AIAA Journal*, Vol. 12, Feb. 1974, pp. 185-190.

[10] Gantmacher, G. R., *The Theory of Matrices*, Vol. I, Chelsa Publishing Co., New York, 1959.